P1.5 RELATIONSHIP BETWEEN LIGHTNING LOCATION AND POLARIMETRIC RADAR SIGNATURES IN A SMALL MESOSCALE CONVECTIVE SYSTEM

N. Lund[1,2,*], D. MacGorman[3], D. Rust[3], T. Schuur[1],
P. Krehbiel[4], B. Rison[4], T. Hamlin[5], J. Straka[2] and M. Biggerstaff[2]

[1]Cooperative Institute for Mesoscale Meteorological Studies, University of Oklahoma and U.S. NOAA/OAR/National Severe Storms Laboratory, Norman, OK
[2]University of Oklahoma, Norman, OK
[3]U.S. NOAA/OAR/National Severe Storms Laboratory, Norman, OK
[4]New Mexico Institute of Mining and Technology, Socorro, NM
[5]Los Alamos National Laboratory, Los Alamos, NM

1. Introduction

A mesoscale convective system (MCS) was observed on 19 June 2004 during the Thunderstorm Electrification and Lightning Experiment (TELEX). The TELEX field program was designed to investigate the relationship between the electrical, microphysical and kinematic structure of a variety of storm types. The field program utilized multiple instrumentation systems to achieve the goals of the project (MacGorman et al. 2008). On 19 June 2004, five systems were in use: the Oklahoma Lightning Mapping Array (LMA), the KOUN 10-cm polarimetric Doppler radar, two 5-cm mobile Doppler radars, balloon-borne electric field meters, and modified NCAR dropsondes. This study utilized all of the data sets available for the convective line.

During the TELEX field program, the Oklahoma Lightning Mapping Array consisted of ten sensors (it has now been expanded to eleven) in central Oklahoma. Each sensor detects 60-66 MHz RF radiation emitted by the lightning channel as it propagates through the storm. A time-of-arrival technique is used to map each source location in time, latitude, longitude, and altitude (Thomas et al. 2004). This analysis technique accurately locates sources in three-dimensions within 100 km of the center of the Oklahoma LMA network and in two-dimensions within 200 km of the center of the network. Additional processing was performed on the LMA data set to group mapped radiation sources into flashes based on the distance and time between sources. The location at which each flash was initiated was then calculated for all flashes that contained more than 10 mapped points. The calculation started with the first 10 points and sequentially eliminated the farthest outliers until the standard deviation was less than 0.5 km or until only 5 points remained.

The KOUN radar is the original prototype for the WSR-88D and has been upgraded to include polarimetric capabilities. The radar is located in Norman, Oklahoma and is approximately 40 km east-southeast of the center of the LMA network. The close proximity of the two systems provides sufficient overlap of the ideal data collection regions within 75 km of the radar. This study focuses on KOUN's southwest quadrant within 70 km of the radar. Full polarimetric volume scans were made approximately every 6 minutes. In addition to analyzing PPIs, a single-pass, isotropic Barnes-type inverse exponential weighting scheme was used to interpolate the data to a cartesian grid thereby allowing the data to be displayed in horizontal and vertical slices (Bruning et al. 2007; Trapp and Doswell 2000).

The two 5-cm wavelength Shared Mobile Atmospheric Research and Teaching Radars (SMART-Rs) were deployed southwest of KOUN. These radars provided dual-Doppler coverage for the southern part of the MCS. Sector scans of the MCS required 2 to 2.5 minutes to complete. The SMART-Rs operated with a 100 km range and a Nyquist velocity of +/- 20 m s^{-1} on this day.

Five balloon-borne electric field meters and modified NCAR GPS dropsondes were launched into four different regions of the MCS: ahead of the convective line, in the convective line, in the the transition zone, and in the stratiform region. The modified dropsonde units measured pressure, temperature, relative humidity, location and wind speed and direction. The electric field meters recorded the vector electric field. This study focuses on the vertical component of the electric field in order to in-

*Corresponding author address: Nicole Lund, Cooperative Institute for Mesoscale Meteorological Studies, University of Oklahoma and U.S. NOAA/OAR/National Severe Storms Laboratory: NSSL/WRDD, National Weather Center, 120 David L. Boren Drive, Norman, OK 73072. E-mail: nicole.lund@noaa.gov

fer the charge distribution near the balloon using the one-dimensional approximation of Gauss's Law (Rust et al. 2005; Bruning et al. 2007).

2. Observations

The MCS formed early in the morning (local time) on 19 June 2004 in an environment characterized by small CAPE (216.8 J/kg) and very weak low-level shear. A cluster of storm cells merged at 1200 UTC to form a convective line without a stratiform region. A fully formed, albeit weak, convective line and stratiform precipitation region formed by 1230 UTC and existed within the study area until 1415 UTC. The cells that initially merged were the most intense of the study period, with the largest reflectivity values and flash rates. After 1415 UTC, the whole system weakened and dissipated. After the remnants of the system had moved outside of our study region, a new convective line formed on the outflow boundary and propagated east as a MCS.

Almost all lightning that was initiated in the MCS clustered in or near individual convective cells and were usually located within two altitude ranges, 3 to 5 km MSL and 7 to 10 km MSL. The MCS went through three distinct phases, defined by the characteristics of lightning flash rates, the altitudes at which lightning was initiated, and radar reflectivity:

- The organizational phase (1000 to 1230 UTC) had large fluctuations in lightning flash rates in response to its transition from scattered storms to an organized line of storms lacking any apparent stratiform region. Lightning was primarily initiated between 8 and 10 km, and as time progressed the VHF source production rate increased.

- The stable MCS phase (1230 to 1415 UTC) was the primary focus of this study. During this period, the MCS had a traditional leading-line, trailing-stratiform appearance on radar. The erratic variations in flash rates decreased, and flash rates steadily increased with time. Lightning was initiated in both the upper and lower altitude ranges; however the upper range continued to produce more than half of the total lightning.

- The weakening MCS phase (1415 to 1600 UTC) was characterized by the apparent break up of the convective line and stratiform region, in conjunction with a dramatic decrease in the total lightning flash rates and in the altitude of the predominant lightning producing range. The decrease in altitude at which lightning was initiated is thought to be due to weakening of the convective line updrafts.

The cellular nature of the locations at which lightning was initiated within the MCS allowed for the investigation of individual cells in the line. Two cells were chosen based on their location with respect to the KOUN radar (within 70 km) and their lightning characteristics. The first cell (a weak, short-lived cell) produced only 12 flashes throughout its lifetime, while the second cell (a large, long-lived cell) produced an order of magnitude more flashes during its lifetime.

The cells focused on here were embedded within the greater MCS storm structure and were not completely isolated. Channels of flashes that were initiated in other cells traversed the focus cells throughout their lifetime and beyond. The VHF source density plots in Fig. 1 show that lightning propagated through both cells at least 10 minutes before any lightning was initiated within the cell and continued at least 10 minutes after lightning production ended. The structure of the VHF source density shows multiple layers of maximum VHF source density. The small, short-lived cell had two layers during peak lightning production, while the large, long-lived cell had three. The smaller cell was dynamically weaker (Figs. 2 and 3). It lasted about 35 minutes and had a maximum reflectivity of 50 dBZ, whereas the larger cell lasted for about 66 minutes and had a maximum reflectivity of 56 dBZ. The lowest and highest altitude VHF source density maxima appear to be aligned with the altitudes at which lightning was initiated (Fig. 1).

The primary difference between the cells lies in the altitude trends of both VHF source density maxima and the altitude ranges at which lightning was initiated. The small, short-lived cell shows a downward trend in both, while the large, long-lived cell shows an upward trend in both until 1255 UTC. This trend is closely related to the polarimetric radar trends shown in Figs. 2 and 3. The upper lightning producing region (roughly 7 to 12 km MSL within each cell) followed the 30 to 42 dBZ maximum reflectivity contours in both cells. The small, short-lived cell began initiating lightning when the 30 dBZ contour peaked in altitude (Fig. 2b) and continued producing lightning as the altitude decreased. In contrast, the large, long-lived cell produced lightning as the 30 dBZ contour increased in altitude (Figs. 3a,b) and produced lightning almost exclusively in the lower altitude region as the 30 dBZ contour decreased in altitude.

The lower lightning producing region (roughly

3 to 6 km MSL within each cell) occurred along the upper edge of the maximum in reflectivity (Z) and differential reflectivity (Z_{dr}) and the minimum in correlation coefficient (ρ_{HV}). These signatures are consistent with the bright band region, which occurs just below the 0^oC level (approximately 4.5 km MSL on this day). If the updraft is too weak to suspend ice hydrometeors, then the bright band will be seen in response to the melting of falling ice particles. Z increases due to an increase in aggregate size in the bright band region, as well as to an increase in the hydrometeors dielectric constant as the aggregate begins to melt and become water coated. These processes also lead to an increase in Z_{dr}. Finally, ρ_{HV} decreases since the sample volume contains a mixture of frozen and liquid hydrometeors (Giangrande et al. 2007).

One of the five balloons launched on this day measured the vector electric field in the convective line. The path of the balloon brought it near the large, long-lived cell, but not inside. Fig. 4 shows the vertical component of the electric field as well as thermodynamic data collected by the radiosonde. Five layers of charge are inferred from the electric field sounding. From top to bottom, the charge density calculated for each of the layers was 0.3 nC m^{-3}, -0.9 nC m^{-3}, 0.4 nC m^{-3}, -0.3 nC m^{-3} and 0.2 nC m^{-3}.

This analysis was compared with the charge associated with the location of mapped LMA sources in the region surrounding the balloon and in both cells we analyzed (Fig. 5). The method used to infer the charge associated with lightning is described by Bruning et al. (2007). All three areas show an upper level positive charge layer above a midlevel negative charge layer, which roughly matches the electric field sounding's upper two charge layers. The convective line and the large, long-lived cell areas show an additional positive charge layer near 4 km MSL. Unfortunately, neither the electric field sounding nor the LMA data can fully diagnose the storm's four-dimensional charge structure. The electric field sounding is limited to the location of the balloon and to the time at which the balloon traversed the atmosphere. The LMA charge analysis is limited to those charge layers which participated in lightning. Therefore, the charge observed by one instrument may not have been observed by the other instrument.

To further investigate lightning relationships with storm structure, the locations at which lightning flashes were initiated were superimposed on polarimetric and dual-Doppler radar data at three different periods in each cell's lifecycle. The patterns seen in both cells were similar for each phase, so we show only one example for each phase. Fig. 6 shows the beginning of lightning production in the small, short-lived cell. Figs. 7 and 8 show the middle and end of lightning production, respectively, in the large, long-lived cell. The locations at which lightning was initiated were overlaid on PPIs and vertical slices. The vertical slices passed through the center of lightning producing regions, which were also near the local maximum in reflectivity. The chosen PPI elevation angles cut through the center altitude at which lightning was initiated for each level. Note that there is an altitude gradient across the PPI plots and the higher elevation plots have a large altitude gradient. During the beginning of lightning production, the lightning producing regions were near the updraft boundary, which had a maximum value of 8 m s^{-1} at 5 km MSL (Fig. 6l). By the end of lightning production, the updraft had transitioned into a downdraft below 4 km MSL (Fig. 8l).

An upper level lightning producing region was present during the first and second stages and was oriented along the upper edge of the high reflectivity region (Figs. 6c and 7c). This region's hydrometeors are best characterized as wet, high-density graupel with Z ranging from 35 - 47.5 dBZ, Z_{dr} ranging from 0.1 - 0.5 dB, and ρ_{HV} ranging from 0.975 - 1. Above this level, the reflectivity drops off quickly to values below 35 dBZ, indicating ice particles in a dry environment. The upper region is consistent with the noninductive graupel-ice electrification mechanism (MacGorman and Rust 1998). During a collision between graupel and ice hydrometeors, charge is transferred between the two hydrometeors (how much and what type of charge each hydrometeor gets is dependent upon temperature and graupel riming rates). Then differential sedimentation of the graupel and cloud ice separates the oppositely charged particles into two regions of net charge. Finally, once enough net charge builds up in each of these two regions, lightning is initiated in the high electric field between the separated charge regions.

A lower level lightning producing region was present during all three cell stages and was oriented along the upper edge of the Z_{dr} column (Figs 6c, 7c and 8c). This region likely contained a mixture of wet, high-density graupel and rain drops undergoing the process of freezing. Z ranged from 37.5 - 57.5 dBZ, Z_{dr} ranged from 0.375 - 1.625 dB, and ρ_{HV} ranged from 0.97 - 0.995. The flashes in this layer were initiated along the top edge of a minimum in ρ_{HV} suggesting that initiation occurred at temperatures slightly colder than 0^oC, which is consistent with the 4.5 km MSL 0^oC level measured in balloon soundings. The freezing of rain drops in this

region may have produced small ice particles (Jameson et al. 1996) that could then participate in the noninductive graupel-ice electrification mechanism.

3. Summary

The 19 June 2004 MCS was a relatively weak, but well sampled system. It was characterized by a bi-level structure in the altitude at which lightning was initiated and by the clustering of lightning production into individual cells. Our analysis focused on two cells. The small, short-lived cell had a decreasing trend in the altitude of VHF source density maxima and the altitude range at which lightning was initiated, while the large, long-lived cell had an increasing trend. However, their similarities far outnumber the differences, indicating that these cells were characteristic of the MCS. The common properties exhibited by the cells are as follows:

- Lightning channels traversed the cells at least 10 minutes before lightning was initiated within the cell.
- There were 2 - 3 maxima in vertical distribution of VHF source density.
- Lightning was initiated within two altitude ranges (3 - 6 km MSL and 8 - 12 km MSL).
- The cells had an upper level positve charge layer above a midlevel negative charge layer, in agreement with the top two layers of charge inferred from the convective line electric field sounding.
- The upper lightning producing regions formed above a local reflectivity maxima.
- The lower lightning producing regions formed near the top of the Z_{dr} column at the top of the melting level.

The regions in which lightning was initiated support the noninductive graupel-ice electrification mechanism theory. The polarimetric data suggest that the upper region was best characterized by wet, high-density graupel and was topped by ice crystals, while the lower region likely contained a mixture of wet, high-density graupel and freezing rain drops which probably produced ice splinters during freezing.

Acknowledgments.

TELEX data acquisition and analysis were supported in part by the National Science Foundation grant ATM-0233268. The authors would also like to thank Eric Bruning and Clark Payne for their contributions in software development and discussions about this study.

REFERENCES

Bruning, E. C., W. D. Rust, T. J. Schuur, D. R. MacGorman, P. R. Krehbiel, and W. Rison, 2007: Electrical and polarimetric radar observations of a multicell storm in TELEX. *Mon. Wea. Rev.*, **135**, 2525–2544.

Giangrande, S. E., J. M. Krause, and A. V. Ryzhkov, 2007: Automatic designation of the melting layer with a polarimetric prototype of the WSR-88D radar. *J. Appl. Meteor. Climatol.*, In Press.

Jameson, A. R., M. J. Murphy, and E. P. Krider, 1996: Multiple-parameter radar oservations of isolated Florida thunderstorms during the onset of electrification. *J. Appl. Meteor.*, **35**, 343–354.

MacGorman, D. R. and W. D. Rust, 1998: *The Electrical Nature of Storms*. Oxford University Press, 422 pp.

MacGorman, D. R., et al., 2008: TELEX: The thunderstorm electrification and lightning experiment. *Bull. Amer. Meteor. Soc.*, In review.

Rust, W. D., et al., 2005: Inverted-polarity electrical structures in thunderstorms in the Severe Thunderstorm Electrification and Precipitation Study (STEPS). *Atmos. Res.*, **76**, 247–271.

Thomas, R., P. Krehbiel, W. Rison, S. Hunyady, W. Winn, T. Hamlin, and J. Harlin, 2004: Accuracy of the lightning mapping array. *J. Geophys. Res.*, **109 (D14207)**, doi:10.1029/2004JD004 549.

Trapp, R. J. and C. A. Doswell, III, 2000: Radar data objective analysis. *J. Atmos. Oceanic Technol.*, **17**, 105–120.

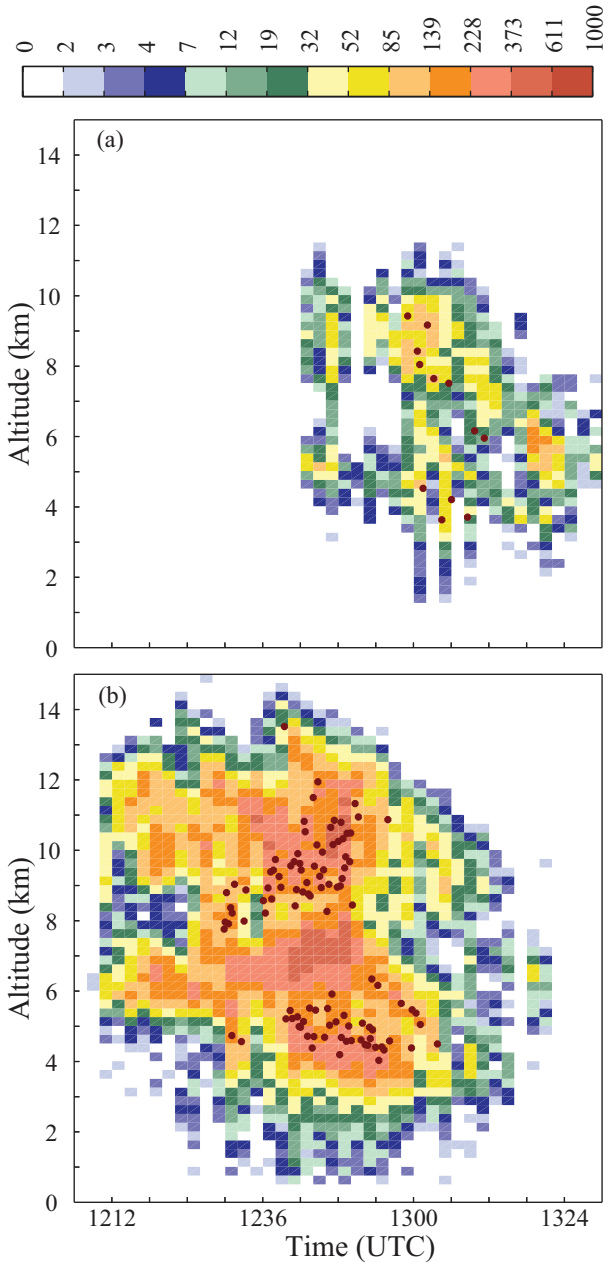

FIG. 1. Time-height plot of VHF source density for all lightning within a 10 km square box centered on (a) the small, short-lived cell and (b) the large, long-lived cell. Densities were calculated by counting the number of sources that fell into each 2 minute by 250 m bin. The locations at which lightning was initiated within each cell are indicated by maroon circles.

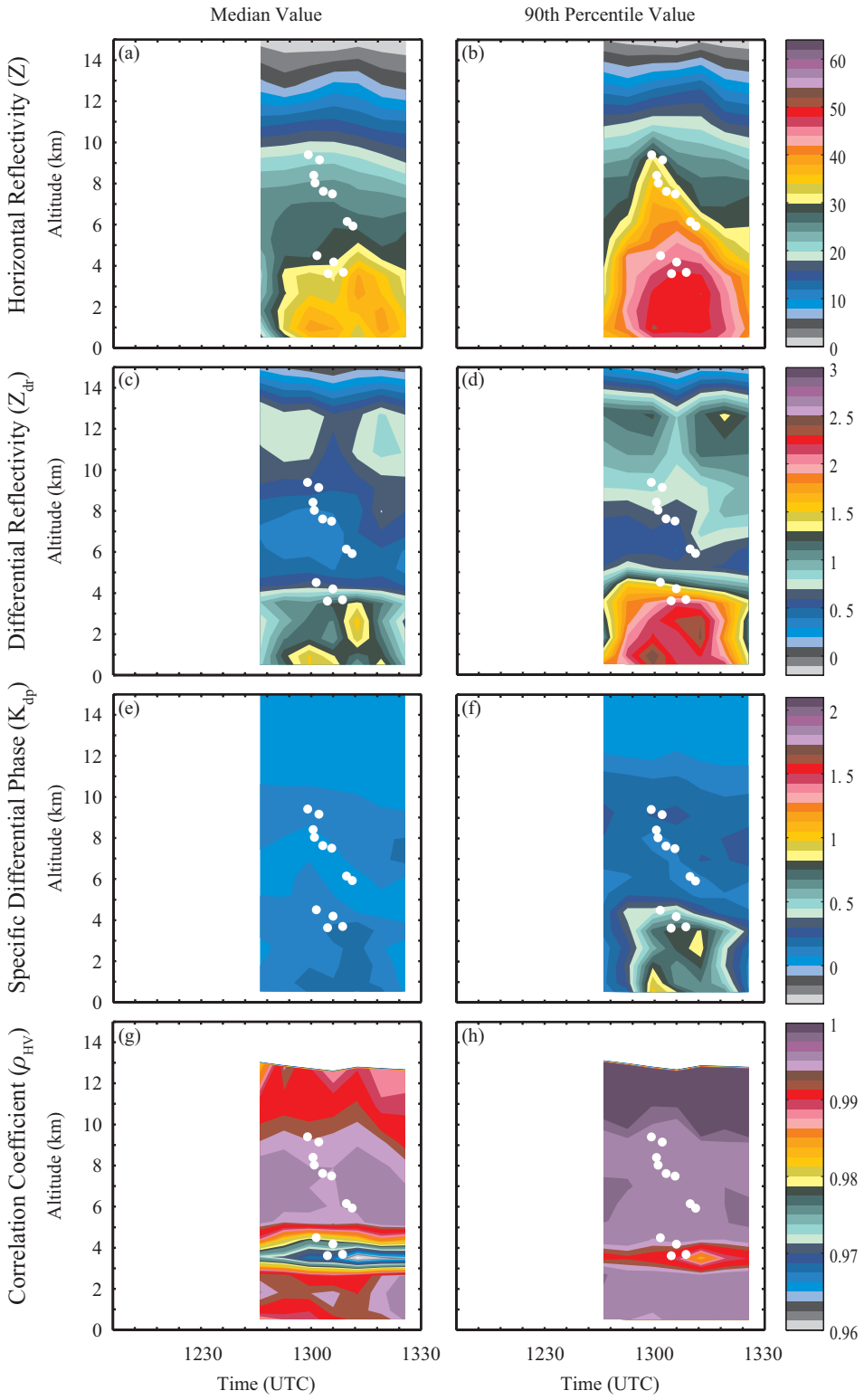

FIG. 2. Median (left column) and 90th percentile (right column) radar values for each radar elevation angle within a 10 km square box centered on the small, short-lived cell. The 90th percentile is calculated by determining the radar value at which 90% of the data occurs below that value for each radar elevation angle. The locations at which lightning was initiated within the cell are indicated by white circles. (a-b) horizontal reflectivity Z, (c-d) differential reflectivity Z_{dr}, (e-f) specific differential phase K_{dp} and (g-h) correlation coefficient ρ_{HV}.

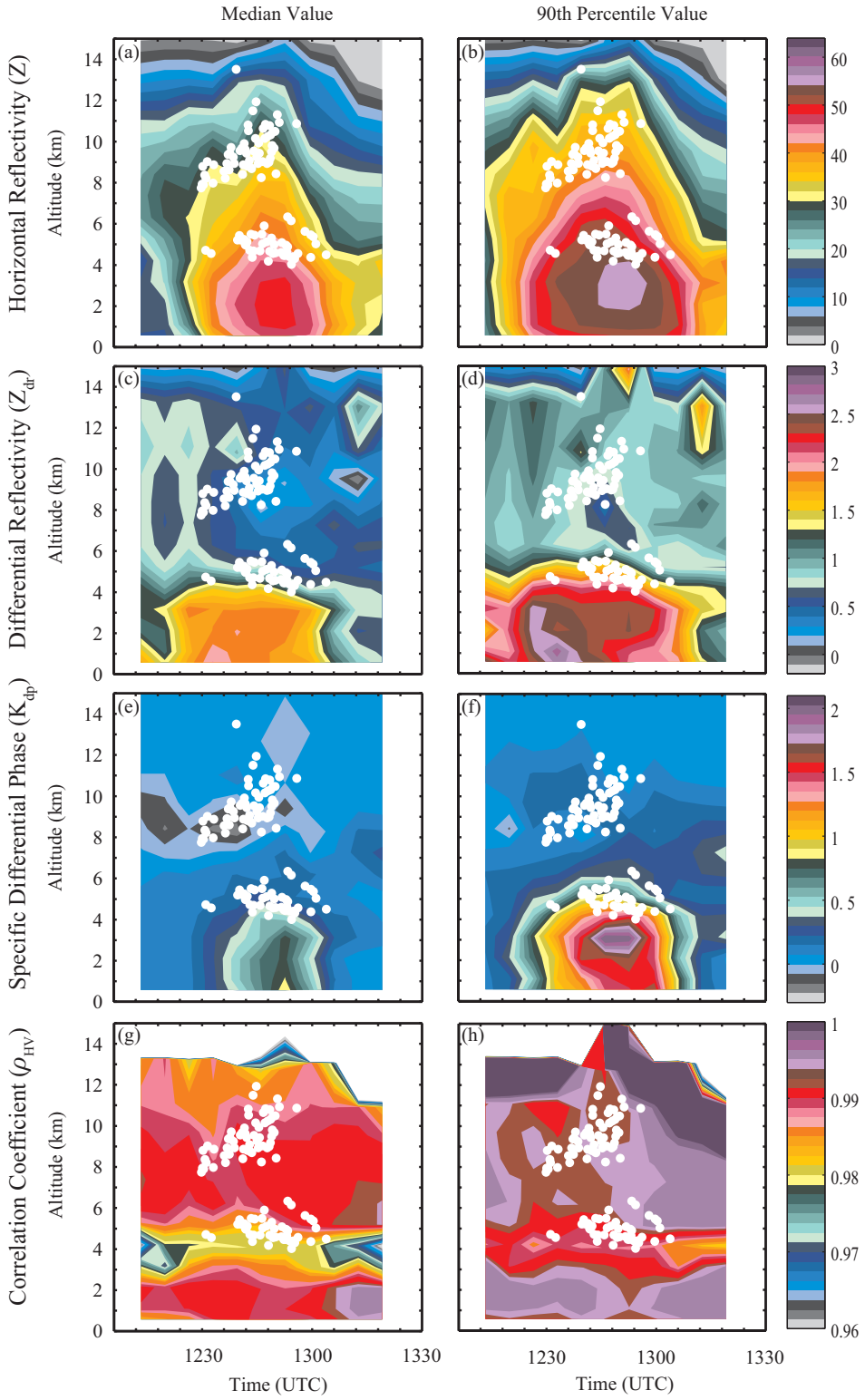

FIG. 3. As in Fig. 2, but for the large, long-lived cell.

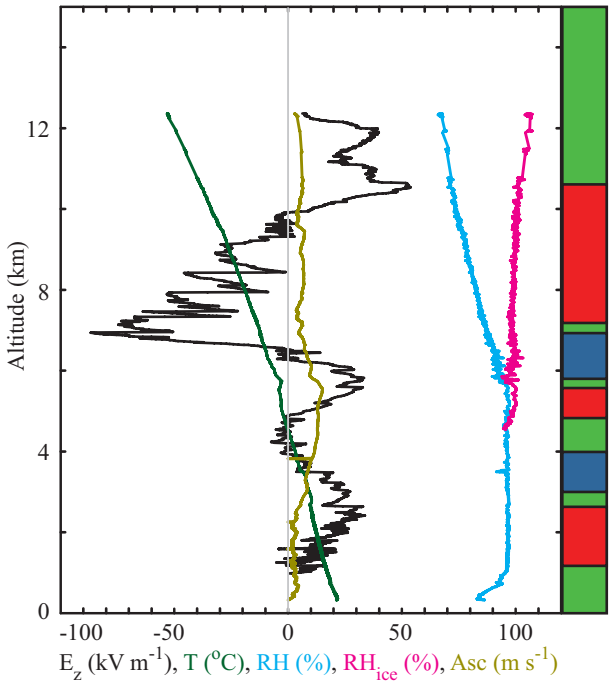

FIG. 4. Electric field and thermodynamic sounding from the convective line. Electric field is shown in black, temperature in green, relative humidity with respect to water in blue, relative humidity with respect to ice in pink and vertical ascent rate in yellow. The colored bar to the right of each figure depicts the charge type measured by the sounding. Red is positive charge, blue is negative charge and green is neutral charge.

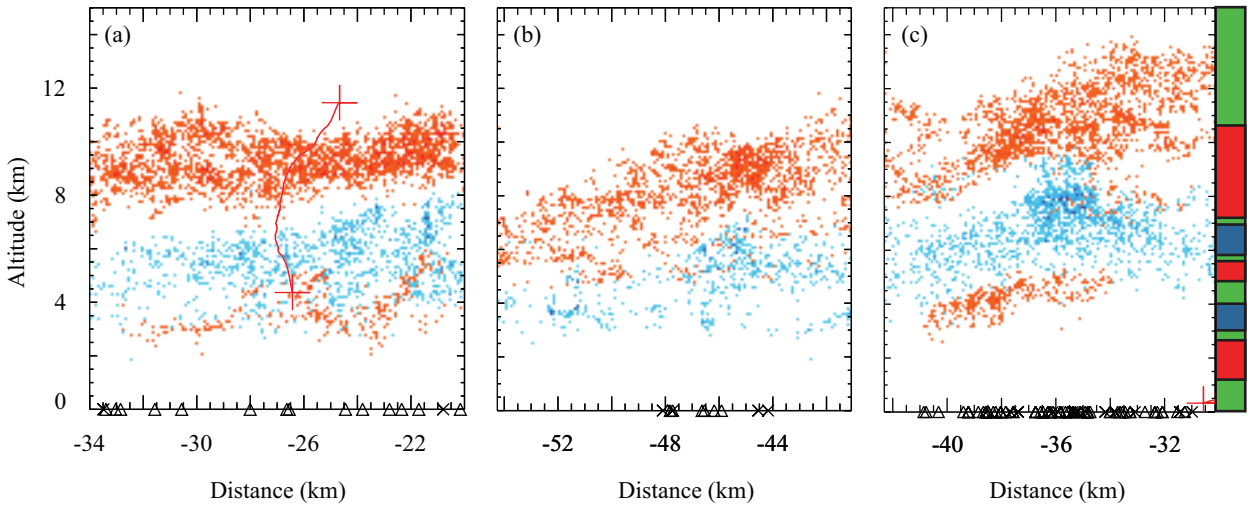

FIG. 5. Charge analysis for (a) the region surrounding the convective line balloon sounding, (b) the small, short-lived cell and (c) the large, long-lived cell. Positive charge is indicated by red dots while negative charge is shown in blue. The colored bar to the right of the figure depicts the charge type measured in the convective line balloon sounding from Fig. 4. Red is positive charge, blue is negative charge and green is neutral charge.

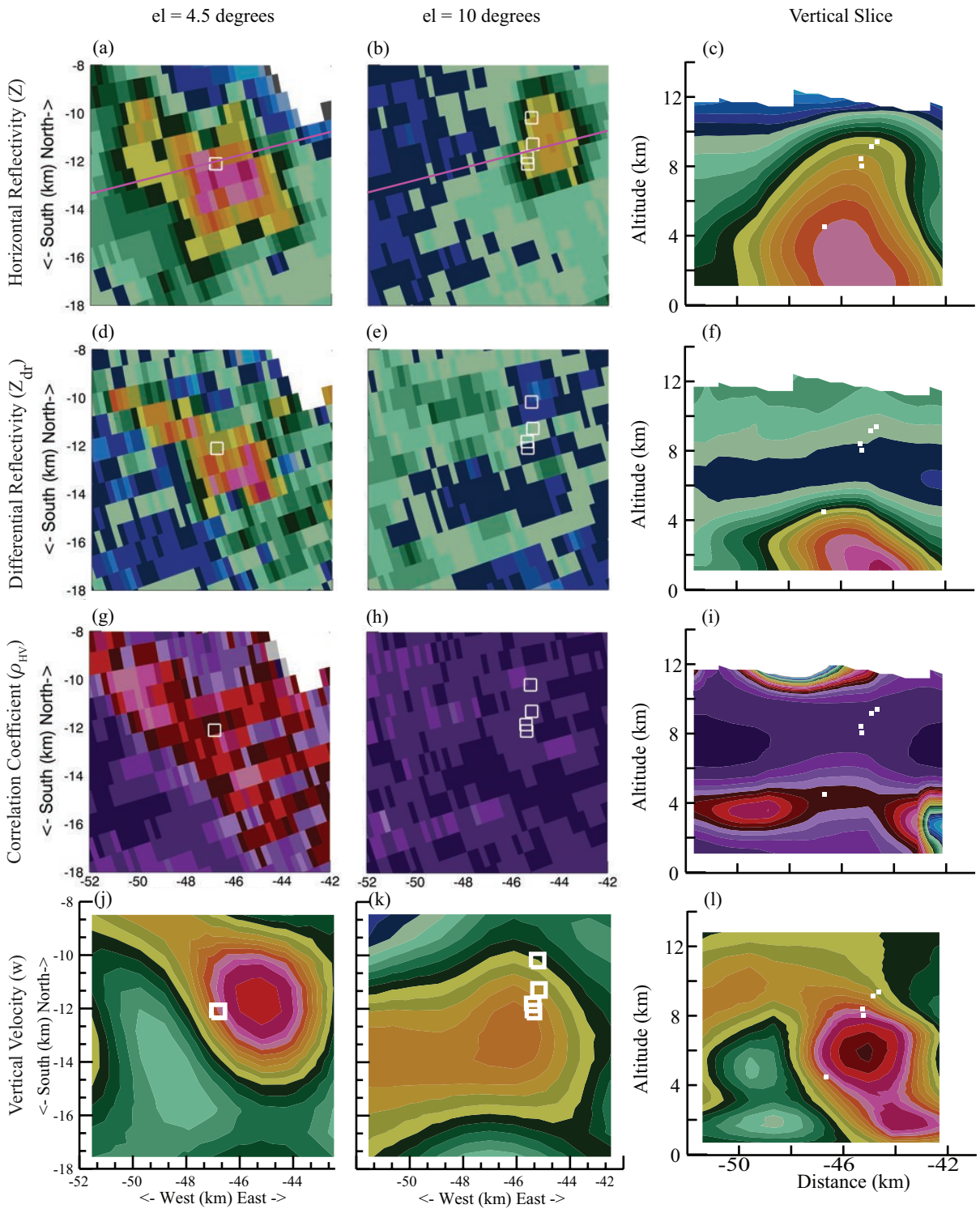

FIG. 6. Interpolated KOUN polarimetric data, SMART-R dual-Doppler data and lightning initiation location (white dots) from the 1256 UTC volume for the small, short-lived cell. The lower elevation (left column) and upper elevation (middle column) PPIs occur near the center of lightning production for each level. The pink line shown in (a-b) indicates the location of the vertical slice shown in the right column. (a-c) horizontal reflectivity Z, (d-f) differential reflectivity Z_{dr}, (g-i) correlation coefficient ρ_{HV} and (j-l) vertical velocity w. Refer to Fig. 9 for color scales.

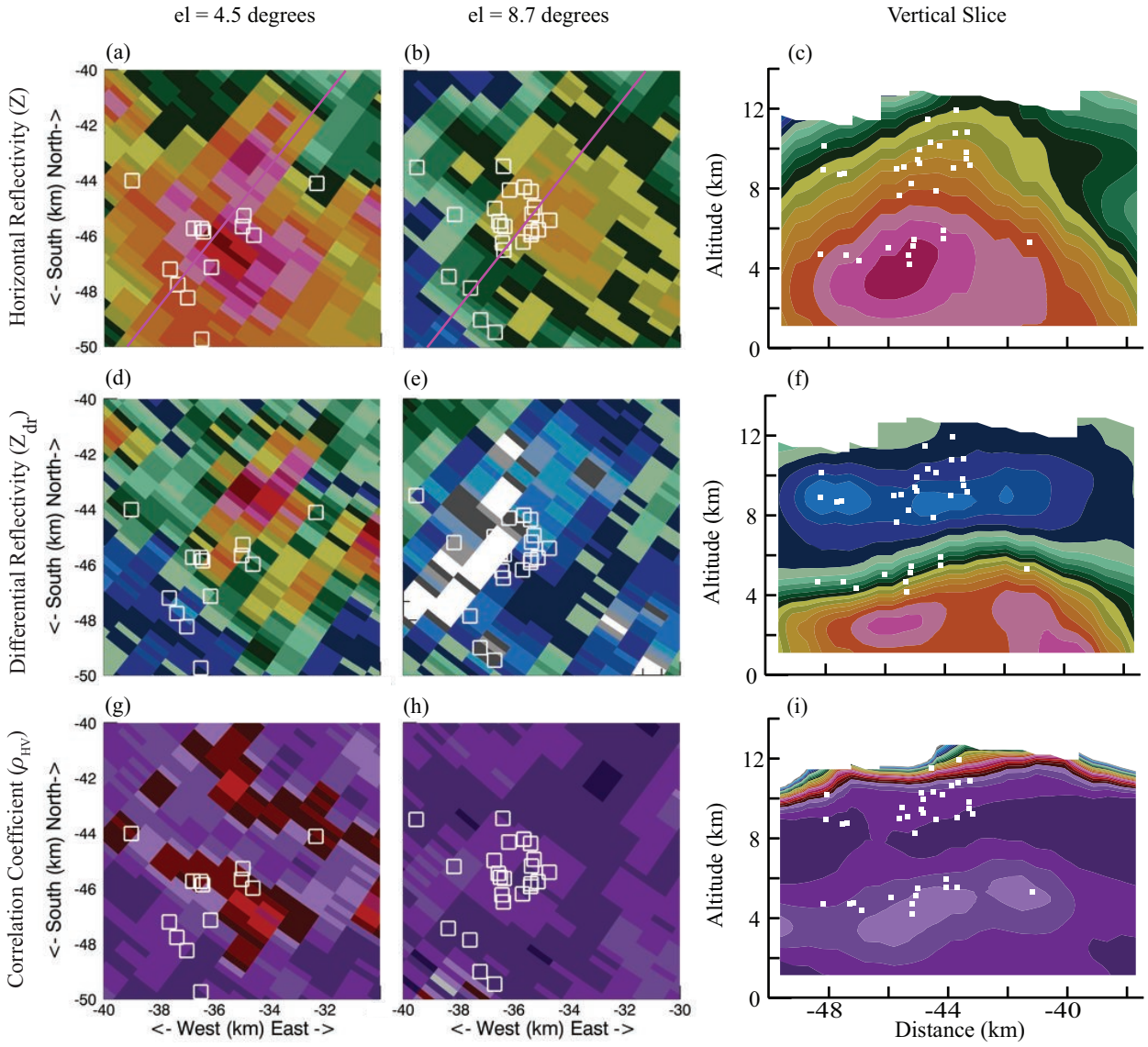

FIG. 7. As in Fig. 6, but for the large, long-lived cell at 1242 UTC. Velocity data was not available for this period.

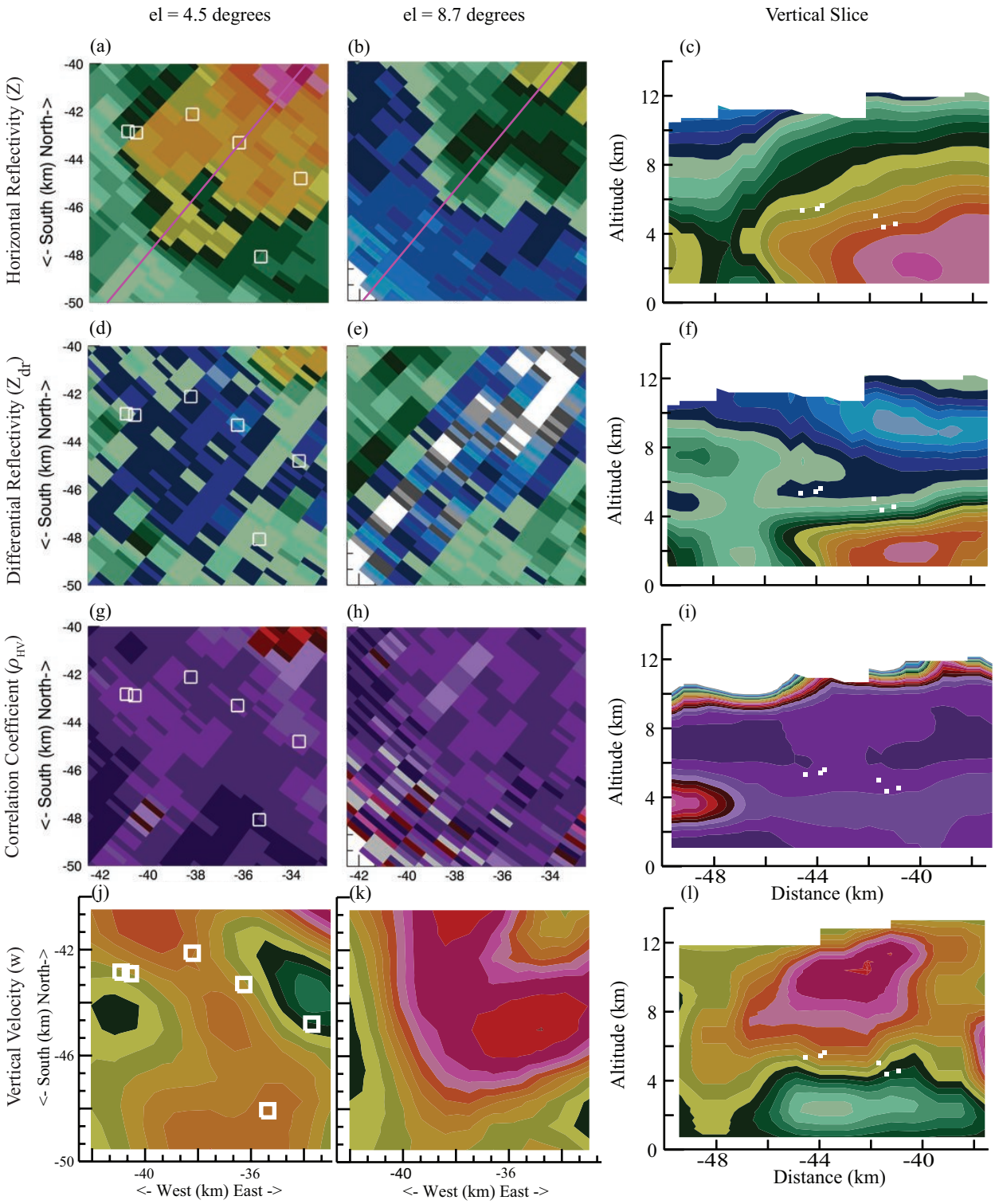

FIG. 8. As in Fig. 6, but for the large, long-lived cell at 1256 UTC.

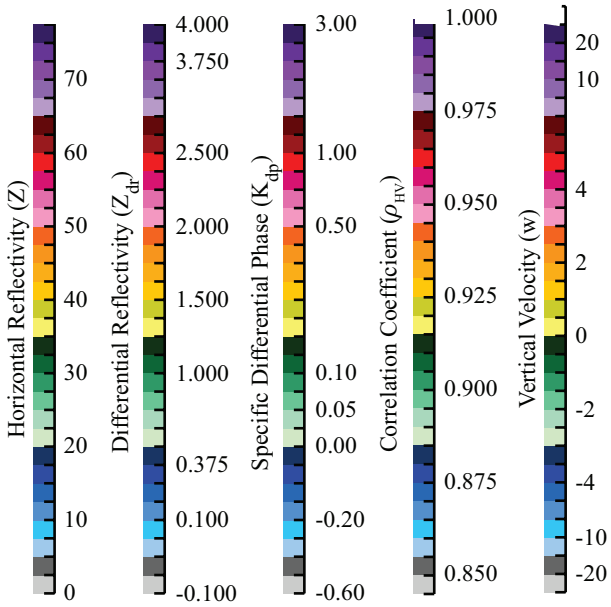

FIG. 9. Color scales for radar PPIs and vertical slices.